

# THEORETICAL AND EXPERIMENTAL INVESTIGATION OF STRINGER PEELING EFFECTS AT STIFFENED SHEARLOADED COMPOSITE PANELS IN THE POSTBUCKLING RANGE

D. Hachenberg <sup>†</sup> and H. Kossira <sup>‡</sup>

Institut für Flugzeugbau und Leichtbau ( IFL )  
( Institute for Aircraft Design and Structural Mechanics )  
Technical University Braunschweig, FR Germany

## Abstract

Results of an experimental and analytical study of the postbuckling behavior of stiffened graphite-epoxy panels loaded in pure shear are presented. The postbuckling response and failure characteristics of the panels are described. Panels with one and two stiffeners were tested. Failure of all panels originated in a skin-stiffener interface region. A method of computing the forces in the interface region between the skin and the stiffener, using a special contact element within a nonlinear finite element code is described. Analytical results correlate well with typical postbuckling test results up to failure. Typical stress distributions within the skin-stiffener interface region were determined analytically. A failure criterion for peeling delamination based on interlaminar forces is presented.

## 1. Introduction

The postbuckling load carrying capacity of primary aircraft structural components, such as stiffened panels, is generally very high. For this reason and in order to reduce structural weight a design philosophy is applied, permitting buckling up to some fraction of the ultimate load. The application of such a postbuckling concept on advanced composite structures is restricted due to the fact, that the most common failure mode of composite stiffened panels in the postbuckling range is stiffener disbonding. This failure often occurs far beyond the potential ultimate load. The amount of work done on postbuckling behaviour of stiffened composite airframe members has mostly been limited to experimental or analytical investigations (e.g. ref. 1 - 7) of the global nonlinear response, not taking into account the effects at the skin-stiffener interface. Some investigators<sup>(8,9)</sup> concentrate on the calculation of the local three-dimensional stresses but do not consider the influence of the global postbuckling deformations. When using two separated models for the global and local analysis<sup>(10)</sup>, the collocation of both systems becomes very difficult in the nonlinear postbuckled regime.

Thus a theoretical and experimental investigation has been carried out to improve the understanding of the nonlinear response of stiffened composite panels with special regard to the disbonding mechanism. Graphite-epoxy Plates, integrally stiffened by one or two T-shaped stiffeners, were tested in a shear-frame. These specimens were

produced with the typical skin thicknesses and stacking sequences of primary structures of transport aircraft. Shear panels usually have at their disposal a very large postbuckling load carrying capacity and stringer disbonding occurs even though the stiffener itself is not under external load. In the experimental program the influence of the stringer torsional and bending stiffnesses on the skin buckling modes and stiffener disbonding effects were studied in a series of tests. Improvements of the interlaminar strength can be reached by pinning the skin-stiffener region of the laminate with steel or titanium pins. Such methods have been examined with the result, that no stiffener disbonding could be observed up to the ultimate load of the plate. Interlaminar material properties as there are peeling strength and critical popoff forces were evaluated by special test specimens and are also described in this paper.

To predict the magnitude of disbonding sensitivity due to skin-buckling it is necessary to analyse the nonlinear response on one side and to cope with three-dimensional effects on the other side. Three-dimensional stresses are responsible for delamination and disbonding, as the interlaminar strengths-properties of laminated composites are rather poor in relation to the inplane ones. In the analytical model a nonlinear Finite Element code is used for postbuckling analysis. Three-dimensional stress distributions at the skin-stiffener interface are determined numerically by the use of a special interface element and thus allow to specify critical regions, wherein the starting point of the delamination is situated. Good correlations could be achieved between the test results and the theoretical predictions. Two failure criteria are presented for stringer disbonding, one based on interlaminar tractions calculated by the interface element and the other one based on postbuckling generalized bending strains.

## 2. Theoretical Investigations

### 2.1 Numerical method

The following buckling and postbuckling analysis of stiffened laminated plates is based on a nonlinear shell theory of the Reissner-Mindlin type (first-order shear deformation plate theory), which is valid over a wide range of thickness ratios and for large deformations but moderate rotations. The nonlinear differential equations of the shell theory are transformed into a set of algebraic equations by means of the finite element method (FEM).

<sup>†</sup> Stress Engineer, Deutsche Airbus GmbH

<sup>‡</sup> Professor of Aircraft Design and Structural Mechanics and Director of the IFL

An in-house (IFL) developed finite element code (*FiPPS* see ref. 14,15), which is based on a mixed variational principle was used to derive a plate element for the idealization of the panel and the stringer cross-section. A detailed description of the application of the mixed variational principle on nonlinear finite element formulations can be found in references 14-16. The major advantage of the used mixed principle is the fact that simple structured element matrices are obtained and only  $C^0$ -continuity is required. According to the threedimensional effects at the skin-stiffener interface a special contact element had to be developed.

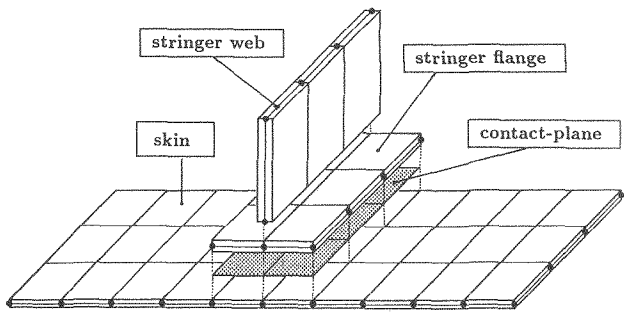
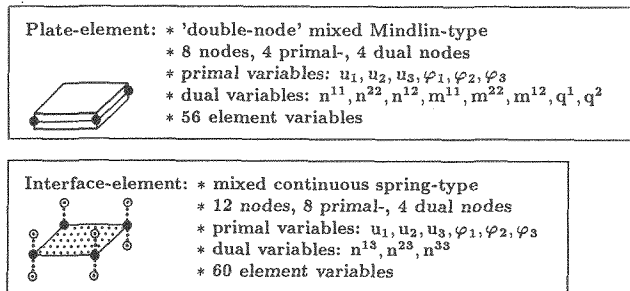


Figure 1: Finite element idealization of a stiffened plate by Mindlin-type plate elements combined with an interface element

### 2.2 Double Node Principle

At the mixed variational principle both the kinematic relations and the equilibrium conditions are satisfied, i.e. both the displacement (*primal*) variables and generalized force (*dual*) variables are given equal importance in the variational process. Thus interpolation functions have to guarantee interelement continuity of not only displacements and rotations but also stress resultants. This fact has limited the application of mixed elements to structures without any abrupt changes in stiffness and unramified ones. The displacement variables may be defined in a global coordinate system but the tractions have to be related to the element reference plane and in the case of a structural ramification - if there is no double-node - a unique association of the stress resultants is not possible. Similar problems arise if a discrete load normal to the element plane is applied. In this case the mixed element formulation effects in a smoothing of the transverse forces discontinuity.

To overcome those lacks of the mixed elements and to make use of their uncontested advantages at nonlinear calculations a decoupling of the stress resultants has to be

performed in those areas of the structure, where abrupt changes occur. This can be reached by attaching the force variables to separated nodes e.g. arranged at the interior of the element and so not taking part in the interelement continuity conditions.

In this study a family of mixed elements was developed with two separated nodes at coincident corner positions (*double-node-element*). One node holds the displacement variables (*primal node*) and the other one the stress variables (*dual node*). While the primal nodes all have to be coupled between the elements, the dual nodes can be coupled or not according to the structural discontinuities or ramifications. The advantages of the mixed formulation thus are retained. The number of unknowns compared to the conventional mixed formulation grows when introducing additional uncoupled dual nodes at the locations of discontinuities. The system band-width of the *double node elements* are larger than those of the conventional mixed elements, which results in higher storage requirements. Moreover an unfavourable numbering of nodes may lead increasingly to indefinite system matrices, which are generally possible when using mixed finite element models requiring special solution procedures<sup>(15,16)</sup>.

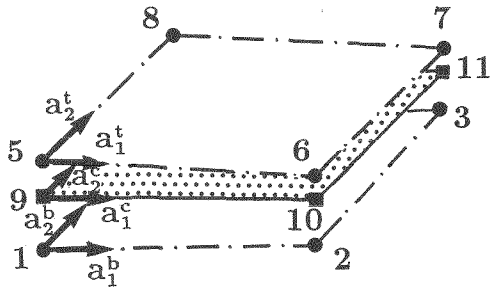
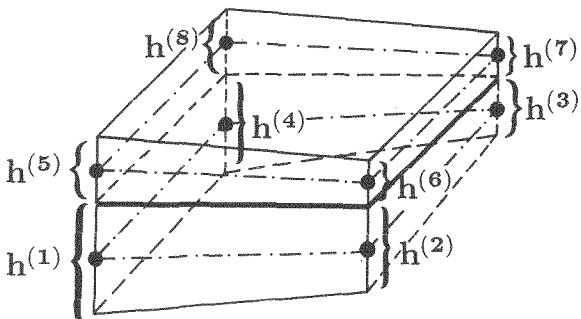


Figure 2: The interface-element as a joint between two plate elements

### 2.3 Interface element

The interface element, which is described in the following is used for the calculation of the interlaminar interactions at a defined interface of the multilayered composite. In the case of a skin-stiffener-idealization the plane of interest is the contact-plane between the skin and the stiffener flange. In displacement models this area can easily be idealized by overlaying two plate elements connecting them to the same nodes and - with regard to their real position - adding an *offset*-vector, which effects their moments of inertia. But as there is only one reference plane and the

variables of both elements are related to it, only plane stress or plane strain conditions can be achieved. On the other hand, if using solid elements, the three-dimensional stresses can be calculated but as the taper fraction must be limited in order to avoid degenerations, the number of elements and unknowns of the global structural model grows up enormously. The aim for the calculation of the skin-stiffener disbonding problem was to have a simple model for the nonlinear global postbuckling analysis and a specific local three-dimensional idealization only at those locations and interfaces, where three-dimensional stresses would effect the stiffener disbonding. Based on the double-node mixed plate-element this was achieved by attaching two different reference systems, one to the elements representing the skin and the other one to those representing the stiffener-flange. Both separated partial systems are then connected by interface elements, which are based on linear spring models<sup>(17)</sup> using similar shape functions as for the connected plate elements.

Considering the 4-node plate element (fig. 2), the thickness of which given at each node by  $h^{(k)}$  and the displacements and rotations by  $u_i^{(k)}$  and  $\varphi_\alpha^{(k)}$ , the displacements of any point on the element-surfaces  $u_i^*$  can be calculated by :

$$\left[ u_i^* \right]_b = \sum_{k=1}^4 \phi^{(k)} \left[ u_i^{(k)} \right]_b - \sum_{k=1}^4 \phi^{(k)} \frac{h^{(k)}}{2} \left[ -a_2^b \ a_1^b \right] \begin{bmatrix} \varphi_1^{(k)} \\ \varphi_2^{(k)} \end{bmatrix}_b \quad (1)$$

$\phi^{(k)}$  are shape functions at the nodes  $k$  and the index  $[\dots]_b$  denotes the upper surface of the bottom plate element of two elements lying one upon another. In a similar way the displacements at the lower surface of the top element ( $[\dots]_t$ ) read:

$$\left[ u_i^* \right]_t = \sum_{k=5}^8 \phi^{(k)} \left[ u_i^{(k)} \right]_t + \sum_{k=5}^8 \phi^{(k)} \frac{h^{(k)}}{2} \left[ -a_2^t \ a_1^t \right] \begin{bmatrix} \varphi_1^{(k)} \\ \varphi_2^{(k)} \end{bmatrix}_t \quad (2)$$

The primal nodes of the bottom plate element are connected to the primal nodes 1 to 4 of the interface element and the primal nodes of the top plate are equal to the nodes 5 to 8 of the interface. The dual nodes of the interface element are numbered from 9 to 12.  $a_1^t, a_2^t, a_1^b, a_2^b$  are unit basic-vectors of the natural coordinate system  $\xi_\alpha$ , which are situated in the reference planes of the connected plate elements. The location of the contact-plane can easily be calculated by simple vektor-operations of the coordinates of the plate element nodes and the discrete corner thicknesses  $h^{(k)}$ . After transforming the surface-displacements  $[u_i^*]_b$  and  $[u_i^*]_t$  into the local coordinate system of the contact plane (index  $c$ ) by using the normal unit vectors  $a_i^c$  we get

$$\begin{bmatrix} u_1^c \\ u_2^c \\ u_3^c \end{bmatrix}_b = \mathbf{a}^T \begin{bmatrix} u_1^* \\ u_2^* \\ u_3^* \end{bmatrix}_b ; \quad \begin{bmatrix} u_1^c \\ u_2^c \\ u_3^c \end{bmatrix}_t = \mathbf{a}^T \begin{bmatrix} u_1^* \\ u_2^* \\ u_3^* \end{bmatrix}_t \quad (3)$$

with

$$\mathbf{a} = [a_1^c | a_2^c | a_3^c] \quad (4)$$

The relative displacements between the points on the upper surface of the bottom element and the lower surface of the

top element in the contact plane  $\Delta u_1^c$  and  $\Delta u_2^c$  ( shear-stress-producing slip ) and normal to the contact plane  $\Delta u_3^c$  ( peel-stress-producing separation ) read:

$$\begin{bmatrix} \Delta u_1^c \\ \Delta u_2^c \\ \Delta u_3^c \end{bmatrix} = \begin{bmatrix} u_1^c \\ u_2^c \\ u_3^c \end{bmatrix}_t - \begin{bmatrix} u_1^c \\ u_2^c \\ u_3^c \end{bmatrix}_b \quad (5)$$

or by means of the matrices  $\Phi_b$  and  $\Phi_t$  containing the shape functions  $\phi^{(k)}$  for the system nodes  $k = 1, 4$  and  $k = 5, 8$  and the vektors  $\mathbf{u}_b$  and  $\mathbf{u}_t$  containing the displacements  $u_i^c$  at the contact-reference plane we get

$$\begin{bmatrix} \Delta u_1^c \\ \Delta u_2^c \\ \Delta u_3^c \end{bmatrix} = \mathbf{a}^T \Phi_t \mathbf{u}_t - \mathbf{a}^T \Phi_b \mathbf{u}_b \quad (6)$$

These relative displacements are corresponding to the transverse tractions  $n_{13}, n_{23}$  and  $n_{33}$

$$\begin{aligned} n_{13} &= k_{13} \Delta u_1^c \\ n_{23} &= k_{23} \Delta u_2^c \\ n_{33} &= k_{33} \Delta u_3^c \end{aligned} \quad (7)$$

or in matrix notation

$$\mathbf{n} = \mathbf{k} \Delta \quad (8)$$

with the decoupled  $3 \times 3$ -property-matrix containing the spring stiffnesses

$$\mathbf{k} = \begin{bmatrix} k_{13} & 0 & 0 \\ 0 & k_{23} & 0 \\ 0 & 0 & k_{33} \end{bmatrix} \quad (9)$$

As there are two separated systems for the stiffener and the skin, delaminations can be modelled very easily by omitting the interface-element or by reducing their spring-stiffnesses. This offers the possibility to regard to impact failures and delamination growth without having to change the finite element model. By the same way the material nonlinearity of the resin-system might be considered through an incremental degradation of the interface spring stiffnesses. In order to capture the stress-peaks at the free edges of the stiffener flanges on the bondline only one row of narrow elements is necessary.

#### 2.4 Failure criterion for stiffener disbonding

The transverse tractions which were calculated with the interface element stand for the interaction between the stiffener and the skin. They can be used therefore as a direct measure for the peeling sensitivity. Based on these tractions a failure criterion was used that reads as follows:

$$\left( \frac{n_{13}^{13}}{n_{cr}^{13}} \right)^2 + \left( \frac{n_{23}^{23}}{n_{cr}^{23}} \right)^2 + \left( \frac{n_{33}^{33}}{n_{cr}^{33}} \right)^2 \leq 1 \quad (10)$$

The strength-values could be evaluated by a T-peel test specimen ( see 3.2 ) in the case of  $n_{cr}^{33}$  and by conventional ILS-tests for  $n_{cr}^{13}$  and  $n_{cr}^{23}$ . As the peeling strength is mainly

dependent on conditions concerning the matrix-system and the curing process ( fiber volume fraction, moisture content, temperature ), all the specimens for the evaluation of strength-values were manufactured and tested under the same conditions as the stiffened plate specimens.

The application of equation 10 is only possible, if the local transverse forces have been calculated by introducing a three-dimensional approach into the global plane-stress analysis of the whole structure. In the practical aircraft design the stress engineer often has to handle very large finite element models for the calculation of the global structural response. Concerning the nonlinear analysis of the whole airframe structure, in some cases it might be not possible further to enlarge the system for the calculation of the peeling stresses. For this reason it could be very usefull to have a failure criterion for disbonding, which only refers to the postbuckled bending deformations. As the magnitude of the peeling stresses depends on the stiffness relations between stringer and skin and can be assumed to be proportional to the bending strains, a failure criterion on the basis of generalized bending strains  $\beta$  [%/mm] (e.g.  $(\epsilon_{upper\ surface} - \epsilon_{lower\ surface})/h$ ) is suggested:

$$\frac{(\beta_{11})^2 + (\beta_{22})^2}{(\beta_{cr})^2} \leq 1 \quad (11)$$

This equation is only valid for stiffened panels with unloaded stiffeners. The critical value of  $\beta_{cr}$  has to be evaluated by peel-test specimens ( table 4 ). In the performed calculations a value of 0.28%/mm was used.

### 3. Tests and Test Results

#### 3.1 Test Specimens

Fifteen specimens were tested in this investigation, manufactured from Thornell T300 8-harness graphite fabric and unidirectional tapes preimpregnated with Fibredux 913C epoxy resin. The typical elastic properties of 3D-lamina ( T300/913C ) are presented in Table 1.

		CFRP T300/913C Prepreg	
		UD-Tape	8H-Satin Fabric
$E_{11t}$	GPa	127.0	69.0
$E_{11c}$	GPa	111.0	60.0
$E_{22t}$	GPa	8.5	64.0
$E_{22c}$	GPa	8.2	56.0
$E_{33t}$	GPa	8.5	8.5
$E_{33c}$	GPa	8.2	8.2
$G_{12}$	GPa	5.2	5.1
$G_{13}$	GPa	5.0	5.0
$G_{23}$	GPa	3.0	3.0
$\nu_{12}$	-	0.28	0.28
$\nu_{13}$	-	0.28	0.28
$\nu_{23}$	-	0.47	0.47

't' denotes tension ; 'c' denotes compression

Table 1: Graphite-epoxy lamina properties

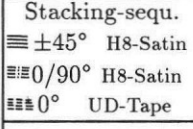
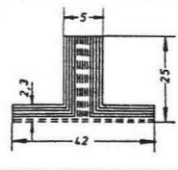
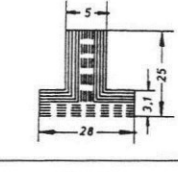
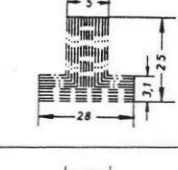
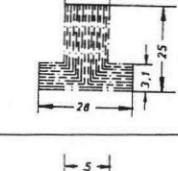
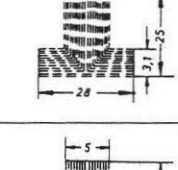
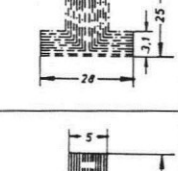
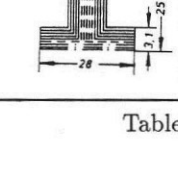
Stacking-sequ. 	Stiffener-Properties				used with panel
	$E_x I_x$ [Nm <sup>2</sup> ]	$E_y I_y$ [Nm <sup>2</sup> ]	$G J_D$ [Nm <sup>2</sup> ]	$\frac{E_x I_x}{G J_D}$ $\Xi$ [-]	
	428	264	28.0	15.3	P <sub>1</sub> & P <sub>2</sub>
	368	188	24.0	15.3	P <sub>3</sub>
	1114	498	4.4	253.2	P <sub>4</sub> ÷ P <sub>8</sub>
	1264	513	3.8	332.6	P <sub>9</sub>
	1798	724	3.9	461.0	P <sub>10</sub> & P <sub>11</sub>
	1330	558	3.9	341.0	P <sub>12</sub> & P <sub>13</sub>
	586	253	25.0	23.4	P <sub>14</sub>

Table 2: Stiffener Characteristics

With respect to maximum shear stiffness the stacking sequence of the skin for all panels was chosen  $[\pm 45]_5$  while the stringer stiffnesses were varied by modifying geometry and stacking sequences (Table 2). This way the influence of different torsional and bending stiffness ratios between the skin and the stiffeners on the peeling effects could be studied. In order to avoid any crippling of stiffener parts and concentrating on the skin-stiffener interface, only T-shaped stringers were used with small flanges but high relative flange thicknesses. Stiffeners and skin were autoclave cured in one shot, i.e. in the same way as it is practiced in Airbus Industry according to a modular design and manufacturing technique. Unidirectional tapes as well as woven material

were used for the stiffener lay-ups for investigating the influence of these combinations on the bonding strength of the skin-stiffener interface. In order to increase the bonding strength of two specimens the interface of which was pinned with steel pins before curing. These pinning was performed by the use of so-called *crowfeet*, which were made by fixing together pairs of usual steel staples. The lengths of the pins were adapted to the thicknesses of the skin and stiffener lay-ups. First the *crowfeet* were pressed through the wet lay-up of the skin positioned at the region where the stiffener should be placed. Being careful enough this could be done without any fiber hurting. Then the skin lay-up was turned around and placed on the aluminium mold, the *crowfeet*-pins now rising some mm above the lay-up. The next step was to lay down the wet stiffener lay-up and pressing the pin-ends into the flange laminate of the stiffeners. The procedure took a lot of time and is done this way not practicable in industrial manufacture. But as an effect of the pinning a remarkable increase of the bonding strength could be observed. The pin-strengthened specimens had no stiffener disbonding up to the failure load of the skin. Some four-point-bending tests down for control purposes as well as similar tests investigated by RICHTER<sup>11</sup> showed, that the bonding strength can be raised by a factor of about 3.0 when using this *crowfeet*-pinning technique.

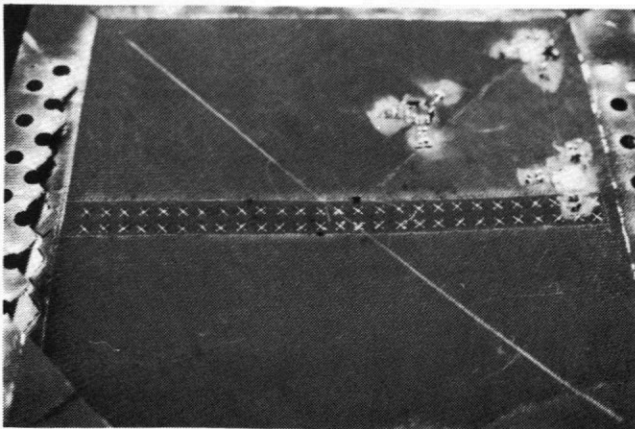


Figure 3: *Crowfeet*-stiffener-fastening : *crowfeet*-heads

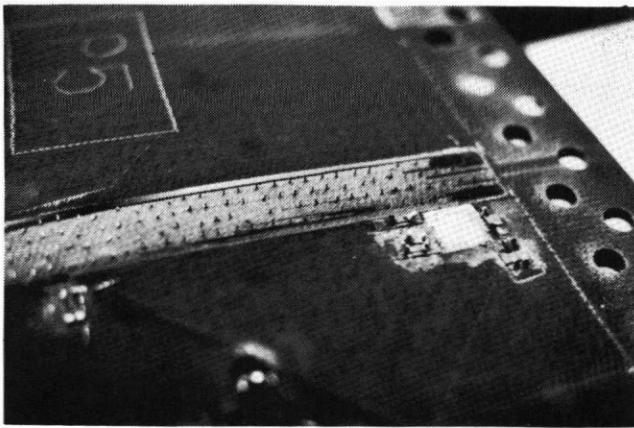


Figure 4: *Crowfeet*-stiffener-fastening : pins of the *crowfeet* after stiffener disbonding due to final failure

### 3.2 Material Properties

Two different peel-test specimens were used for the evaluation of interlaminar properties according to the two critical regions, one at the center of the skin-stringer bonding plane and the other one at the edge of the stiffener flange (figure 5).

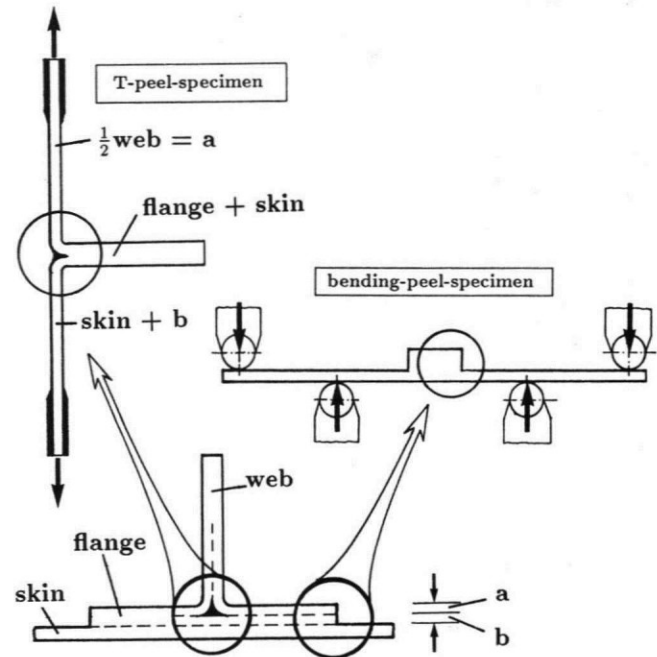


Figure 5: Extraction of peel-test-specimens

A T-peel test specimen represents half the thickness of the stringer web angled to the flange which is joined to the skin laminate in one shot curing process. This specimen stands for a loading condition normal to the interface. Popoff-forces are produced in the postbuckling state by differences in bending stiffness between the stringer and the skin normal to the axis of the stringer. Up to the initial failure the T-test specimen is under pure peeling load, so the evaluated failure load is a measure for the peeling strength. Table 3 shows the results of a series of T-peel tests. It should be noticed, that the peeling strength is not rate independent. In the analytical study a strength-value of  $70 \frac{N}{mm}$  was used.

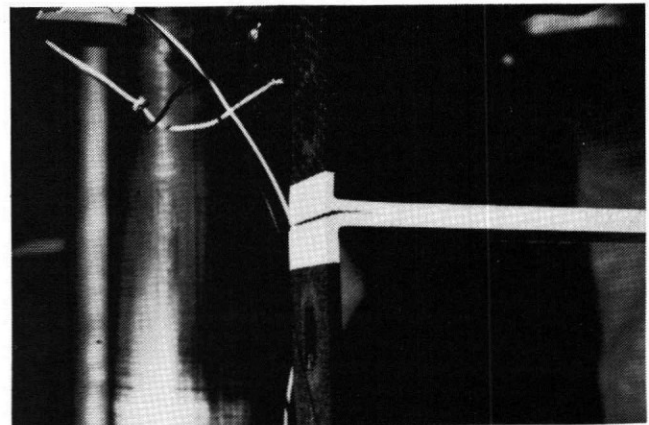


Figure 6: T-peel-test specimen after initial failure

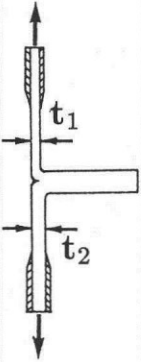
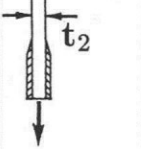
T-peel-test specimens (co-cured)	N	Stacking sequence 913C/T300	specimen		size b [mm]	Initial Crack $\frac{P_{cr}}{b} \left[ \frac{N}{m} \right]$
			$t_1$ [mm]	$t_2$ [mm]		
	7	$t_1 : [\pm 45]_{3s}$ $t_2 : [\pm 45]_{4s}$ fabric H8 Satin	2.1	3.0	30.	74.1 (V <sub>1</sub> ) (s=6.6)
						63.0 (V <sub>2</sub> ) (s=16.5)
	8	$t_1 : [0/90]_{3s}$ $t_2 : [0/90]_{4s}$ fabric H8 Satin	2.0	3.0	30.	64.1 (V <sub>1</sub> ) (s=3.12)
						63.3 (V <sub>2</sub> ) (17.7)
V <sub>1</sub> : testing-rate: 5.0mm/min V <sub>2</sub> : testing-rate: 0.5mm/min			N: batch quantity s: standard deviation			

Table 3: Results of T-Peel-test specimens

The second type of peel-tests was performed by bending peel specimens, which represent the stress state at the edge of the stiffener flange when the skin buckles. Differences in bending and torsional stiffnesses between the skin and the stringer flange along the axis of the stiffeners cause shear and normal peel forces in the postbuckling state. The bending peel test specimens were used for the verification of the analytical model. Results are shown in table 4.

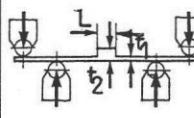
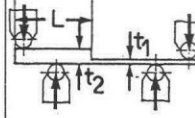
bending-peel specimen (co-cured)	type A	type B
4-point-bending-test		
Quantity	8	9
stiff. length L	45 mm	150 mm
spec. width b	35 mm	40 mm
thickness $t_1$	3.6 mm	2.1 mm
thickness $t_2$	9.0 mm	8.0 mm
specimen lay-up	$[0/90]_{5s}$	$[0]_8$
stiff. lay-up	$[0/90]_{7s}$	$[0]_{11}$
stiffn. at $t_1$ $E \cdot I_x$	8.5 Nm <sup>2</sup>	3.9 Nm <sup>2</sup>
stiffn. at $t_2$ $E \cdot I_x$	253 Nm <sup>2</sup>	566 Nm <sup>2</sup>
critical bending: $m_{cr} = M_{cr}/b$	485 Nm/m	415 Nm/m
critical value of: $\beta_{cr}$	0.28 %/mm	0.30 %/mm

Table 4: Results of bending-peel-tests

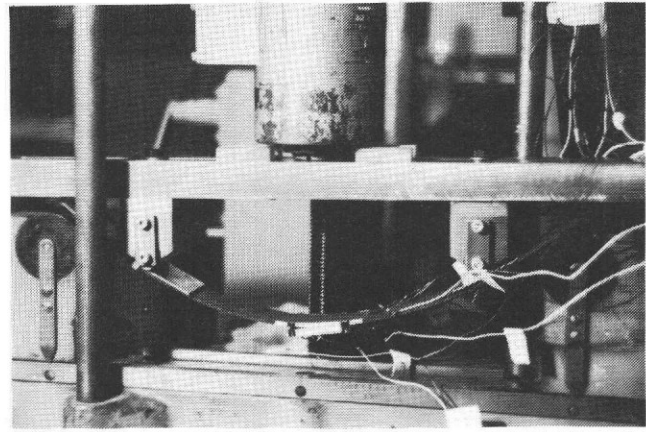


Figure 7: Bending-peel-test-specimen after initial failure

### 3.3 Test setup

The inplane shear testing of the stiffened panels was performed with the same picture-frame fixture that has been used in former investigations with unstiffened flat plates<sup>(12)</sup> and shallow curved panels<sup>(13)</sup>. This shear-frame is composed of four pairs of back-to-back rigid steel edge members connected with high strength pins. These pins are positioned with their center lines coincident with the corners of the test section of the panel. By splitting the corner pins they do not extend through the test panel. Their location at the test section corners prescribes correct picture frame kinematics to insure proper shearing load introduction into the panel test section by applying a tension load along one diagonal of the frame. The specimen edges, which were bolted to the picture-frame members, did not have any reinforcements and were prevented from sliding by added sandpaper.

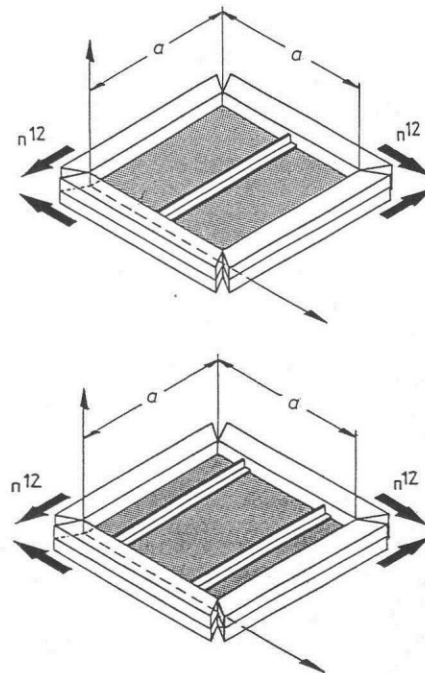


Figure 8: Schematic drawing of a rigid fixture-frame-setup for the shear testing of stiffened plates

The tension load was applied by a 200 kN hydraulic testing machine and the angle of shear of the loaded test specimens was determined by using several inductive displacement transducers for measuring both the elongation along the tension-diagonal and the shortening along the compression-diagonal. The initial geometric imperfections of the specimens and the out-of-plane buckling displacements along the compression-diagonal were monitored by a deflection transducer which was attached to a carriage running on a slideway. Electrical resistance strain gauge rosettes positioned on both surfaces of the specimens were used to measure normal and shear strains. The uniaxial tension loading of the picture-frame fixture was applied slowly in an incremental way up to the total failure of the specimen. At each load increment the angle of shear, the out-of-plane displacements and the strains at three significant positions were measured and recorded on magnetic tape. The stiffener separations could be monitored by optical inspections or in one case by ultrasonic scanning of the skin-stiffener interface region.

### 3.4 Test results

The shear tests with single stiffened panels showed two different buckling modes depending on local imperfections and the bending and torsional stiffnesses of the stringers. If the bending stiffness of the stringer was low ( stacking sequence  $\pm 45^0$  ) the panel tended to buckle into a mode-shape similar to that of an unstiffened panel with reduced amplitude in the stiffener area. This buckling mode can be regarded as symmetric to the center-point of the panel and is therefore indicated with an 's' at the following considerations. The next higher buckling mode could be observed when panels were tested with an increasing share of 0-degree layers in the stiffener cross-section, which caused higher bending but reduced torsional stiffness. It is an antimetrical mode-shape with sinusoidal amplitudes along both panel diagonals ( indicated with an 'a' ) and it tends towards a snap-through into the first symmetric mode. This happened with one of the tests specimen (  $P_4$  ) and could be proved analytically, too. The results of all tests are listed in table 5.

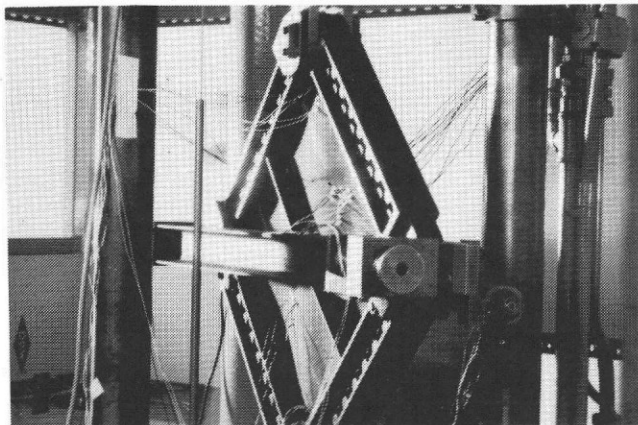


Figure 9: Single-stiffened shear panel in the postbuckling range before stiffener disbonding

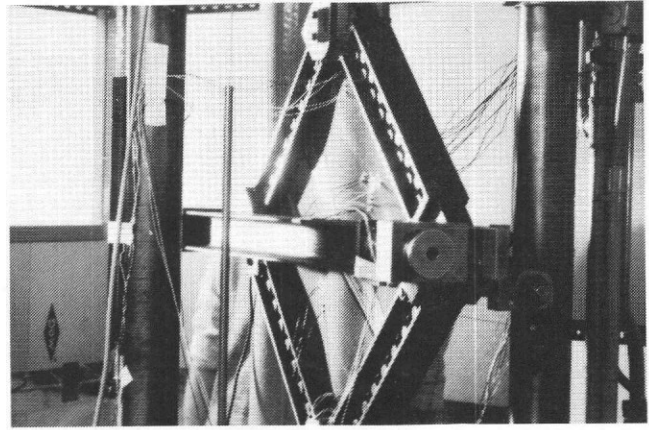


Figure 10: Single-stiffened shear panel in the postbuckling range shortly after stiffener disbonding

The disbonding of the stiffener at the single-stiffened panels happened abruptly and totally with a loud popping noise. After the disbonding a tension field built up and the specimen could further be loaded until final failure. But this final failure load was not very far above the stiffener disbonding load ( Table 5 ). The effect of the explosive stiffener disbonding can be seen as a result of a symmetric distribution of peeling stresses along the stringer bonding line (Fig. 15).

Panel Nr.	$h_m$ [mm]	Fail.-load [kN]	Buckl.-load [kN]	$\tau_B$ [ $\frac{N}{mm^2}$ ]	$\tau_{cr}$ [ $\frac{N}{mm^2}$ ]	$F_{cr(Str.)}$ [kN]
Unstiff. reference Plate						
$P_0$	1.97	166	20	158	19	—
Plates with one stiffener						
$P_1$	1.98	163	60	146	54	156
$P_2$	1.93	181	60	168	56	—
$P_3$	2.04	186	60	173	56	157
$P_4$	1.94	161	55	147	50	148
$P_5$	1.94	152	55	138	50	—
$P_6$	1.98	189	55	168	49	—
$P_7$	1.98	170	55	152	49	—
$P_8$	2.14	160	70	132	58	159
$P_9$	2.08	175	55	149	47	—
$P_{10}$	2.06	184	60	158	47	149
Plates with two stiffeners						
$P_{11}$	2.20	189	70	151	56	159
$P_{12}$	2.38	—	75	—	56	—
$P_{13}$	2.30	184	60	142	46	144
$P_{14}$	2.27	182	55	142	43	158

Table 5: Summary of test results

Another type of mechanism could be observed at the double-stiffened panels, where the buckle mainly affected only one part of the stiffener-region. So the failure mode at these panels was a partial delamination of one or both of the stringers starting at the unconnected ends and growing with increasing load. The total disbonding mostly did not happen before the final failure of the whole panel.

#### 4. Results and Discussion

As the used fixture frame setup was very stiff compared to the tested panels, the engineering angle of shear  $\gamma$  was used as loading parameter for comparison of experimental and analytical results, thus not having to consider the influences of friction of the frame-joint. In the analysis the load was introduced by shearing displacements (displacement controlled) and during the tests the angle of shear was directly measured. As described the out-of-plane displacements (buckling amplitude) were measured along the compression-diagonal of the test panel. Figure 11 shows such measurements for test-panel  $P_4$ , which was the only specimen showing a 'snap-through' from the second mode shape into the first one without stiffener disbonding.

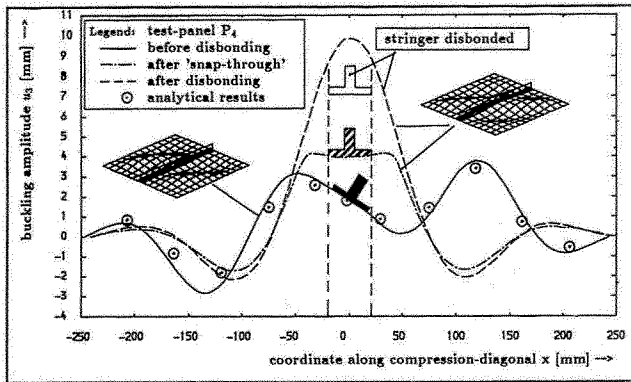


Figure 11: Buckling amplitude along compression diagonal for test panel  $P_4$  at three different load levels

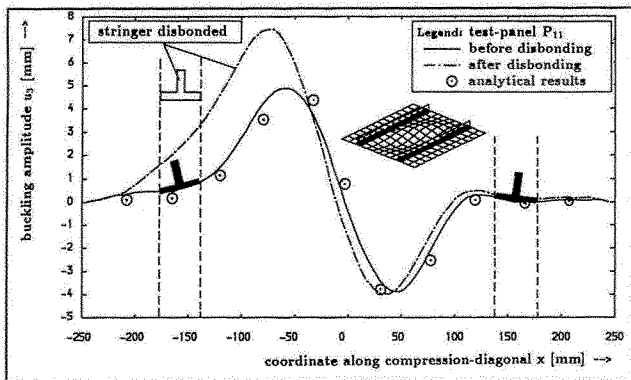


Figure 12: Buckling amplitude along compression diagonal for test panel  $P_{11}$  at three different load levels

The slopes of the curves in the middle section show that the higher mode-shape causes a torsional deformation of the stringer with small bending while the first mode-shape leads to a higher bending amplitude without any torsion. The total disbonding of the stringer results in the formation of a diagonal tension field with double the

amplitude. The panels with two stiffeners behaved much less dramatically in the test (fig. 12). The partial disbonding of one stiffener causes a slightly altering buckling mode shape with increasing amplitude at this panel-section. The analytically determined out-of-plane deformations correlate well with the test results up to the initial failure. This can be seen in figures 13 and 14. Fig. 13 representing test specimen  $P_6$  (no stiffener disbonding due to 'crowfeet'-fastening) and fig. 14 representing test specimen  $P_{10}$  with antisymmetrical mode shape and stiffener disbonding at 0.4 degree shearing angle. The comparisons have been done for three specific points of the panel, one exactly at the center of the panel and the stringer (subscript  $m \Rightarrow \nabla$ ) and one on the compression diagonal in the middle of the buckling field (lefthand field: subscript  $l \Rightarrow \odot$ ; righthand field: subscript  $r \Rightarrow \diamond$ ). Differences in the prebuckled area are due to an incomplete idealization of the imperfections. In the analytical model a 1-cos-imperfection mode was assumed for the whole panel and overlaid by two separated 1-cos-modes for each field area.

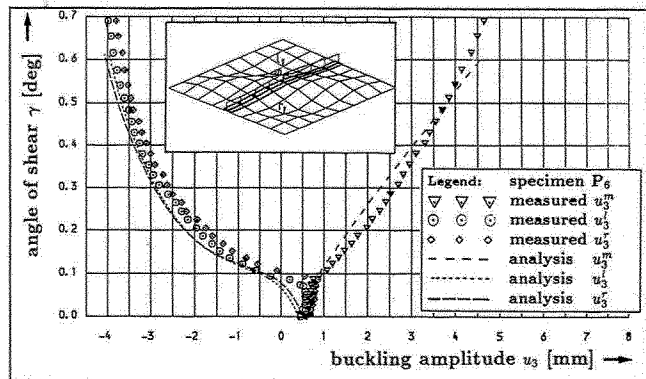


Figure 13: Buckling amplitude as a function of shearing load for panel  $P_6$  at three specific points

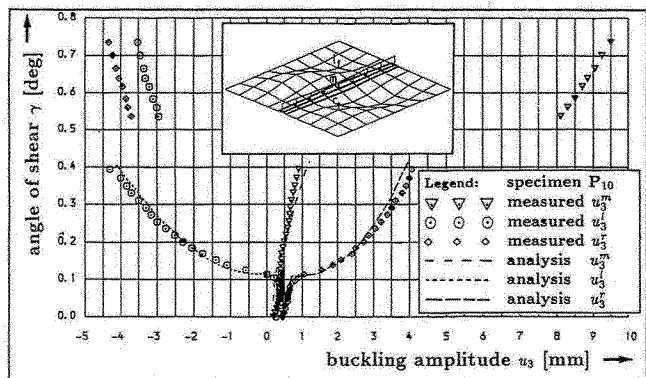


Figure 14: Buckling amplitude as a function of shearing load for panel  $P_{10}$  at three specific points

The following figures (15-17) show the results produced by the interface element. The transverse tractions  $n^{13}$ ,  $n^{23}$ , and  $n^{33}$  have been plotted against each node-line of the element-mesh at the skin-stiffener interface section. For



a better illustration the mesh-length in the direction of the transverse axis has been magnified by a factor of 2.5. The corresponding buckling mode-shape can be seen on top of the figures. Figure 15 shows the results of the first mode shape. The  $n^{13}$ -distribution is directly affected by relative displacements normal to the stiffener axis and  $n^{23}$  by relative displacements along the stiffener axis.  $n^{13}$  reaches maximum values just at the location, where the buckle transmits through the stringer section, while  $n^{23}$  achieves the maximum at the sections with the largest skin curvatures at the flanges of the buckle. The normal traction  $n^{33}$  are caused by the above mentioned *Pop-Off-Force* at the center just beyond the stringer-web, but it becomes negativ (preventing the peeling) towards the free edges of the stringer flanges. The symmetry related to the center is obvious for all tractions at this mode shape.

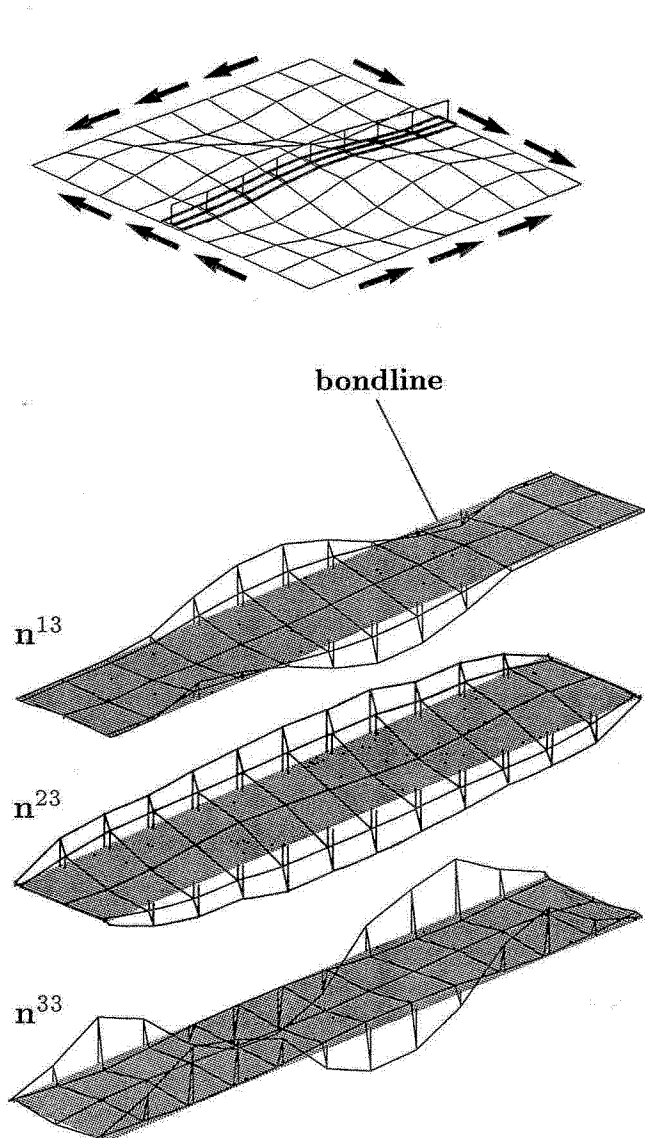


Figure 15: Distribution of interlaminar tractions for a symmetric postbuckled mode shape

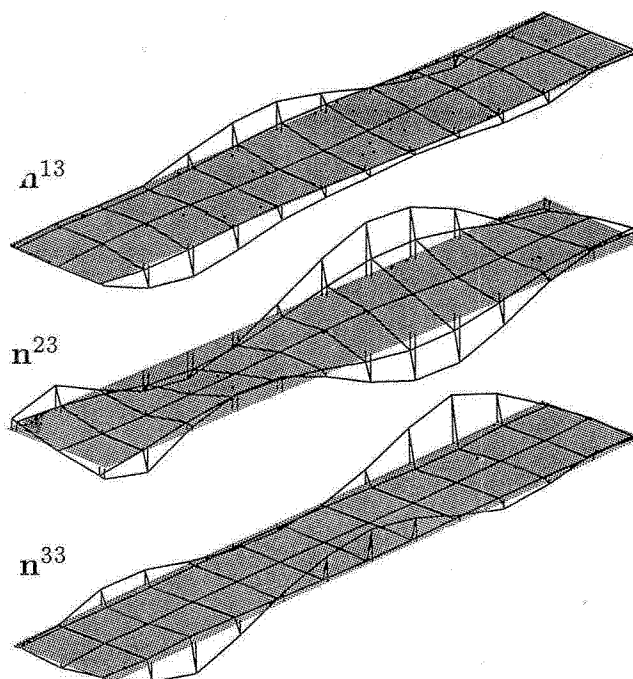
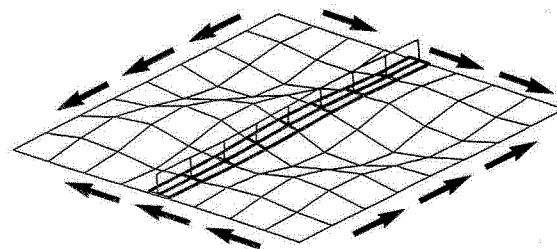


Figure 16: Distribution of interlaminar tractions for an antimetrical postbuckled mode shape

If the panel buckles into the higher second mode shape, the distribution of transverse tractions becomes quite different ( fig. 16 ). The  $n^{13}$  maxima are less significant and the  $n^{23}$ - distribution is much more 'filled', which seems to be the reason for a greater disbonding sensitivity of this mode shape.

Comparing the distributions of the two single-stiffened panels with those of the dual-stiffened ones (fig. 17), it is easy to recognize that the maximum values are reached at the stiffener edges near the tension diagonal of the panel. These are exactly the locations, where the partial disbonding of the stringers was initiated during the tests.

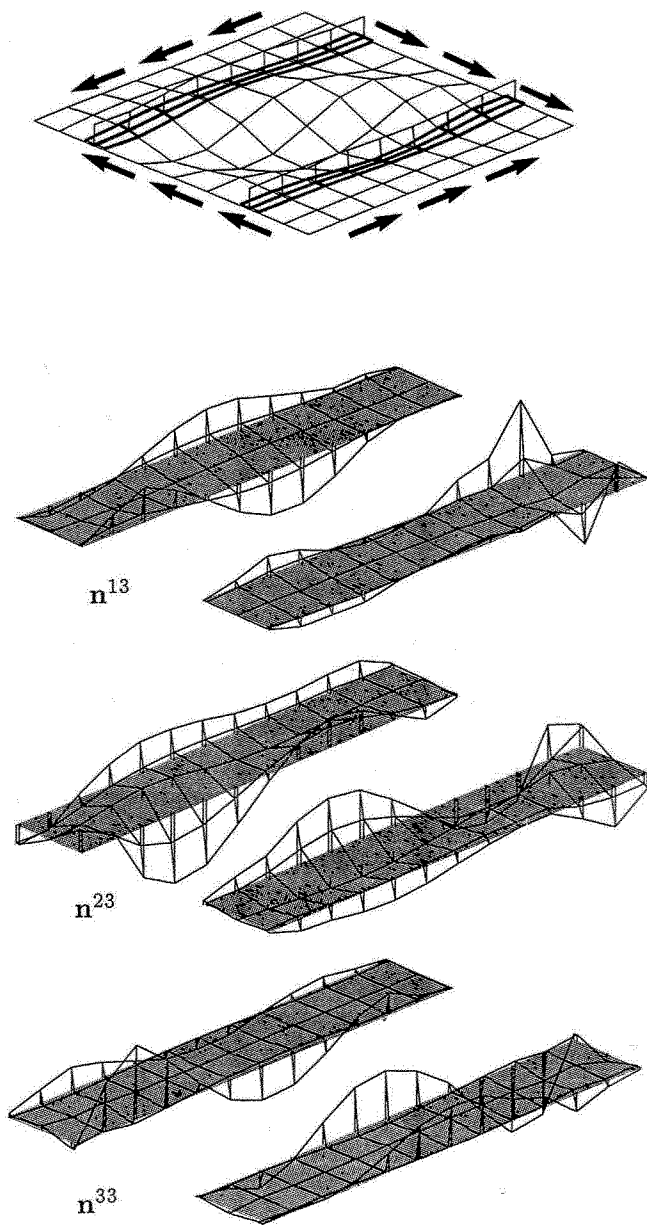


Figure 17: Distribution of interlaminar tractions at the dual-stiffened panels

The last two figures 18 and 19 show the calculated distribution of the generalized bending strains along the stringer bondlines at both sides of the flanges and at a load level just before the disbonding happened at the corresponding test specimen. The bending strains both reach the assumed critical value of 0.28%/mm which means that they will satisfy the failure criterion formulated in equation 11. At this load level the alternative failure criterion ( equ. 10 ) based on the interlaminar tractions is satisfied, too.

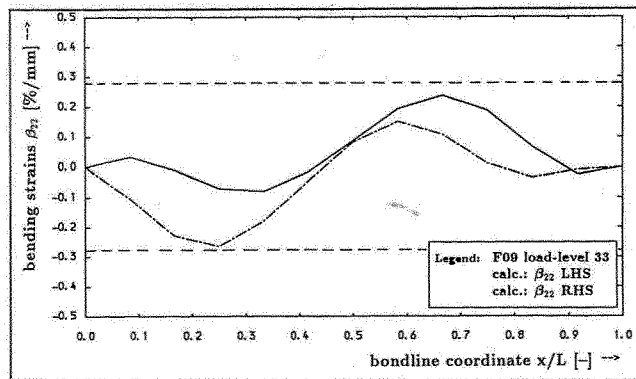


Figure 18: Distribution of generalized bending strain  $\beta_{21}$  along the stiffener bondlines

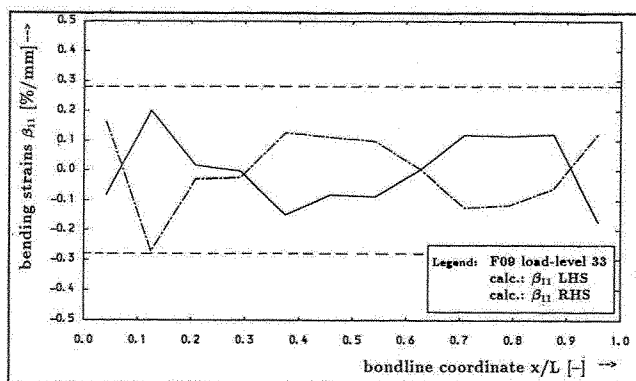


Figure 19: Distribution of generalized bending strain  $\beta_{22}$  along the stiffener bondlines

## 5. Conclusions

An experimental and theoretical investigation was conducted to study the postbuckling response of flat stiffened graphite-epoxy shear panels with special regard to the disbonding failure characteristics due to postbuckled out-of-plane deflections. The test results have demonstrated the very high postbuckling load carrying capacity of cured stiffened panels under shear load inspite of the limitation caused by the stiffener disbonding failure. There was no stiffener disbonding below a load-factor of at least 2.3 times the critical buckling load. An improvement of the stiffener peeling strength by transverse sticking will increase the disbonding load up to a level which is higher than the ultimate load of the skin.

The presented analytical model proved to be capable for the analysis of the global nonlinear response as well as for the determination of the interlaminar effects at the skin-stiffener interface. The additional expenses for the calculation of the threedimensional stresses at the interface are small compared to an overall threedimensional approach.

As good correlations could be achieved between the analytical and the experimental results the authors are encouraged to use the model for the analysis of stiffened panels under different loading conditions, e.g. compression or compression and shear. When compression loads are introduced into the panel, the stringer will carry part of the loading and this will increase the level of the peeling stresses related to the transverse shearing stresses. The problem of stiffener disbonding therefore becomes still more significant with compression loading.

## 6. Acknowledgements

The investigation was performed at the Institut für Flugzeugbau und Leichtbau (IFL) and supported in a joint-venture by the Deutsche Airbus GmbH ( former company: Messerschmitt-Bölkow-Blohm GmbH, Transport-Aircraft-Section ), and by the *BMFT* of the FRG.

## 7. References

- [1] VESTERGREN, P.; KNUTSSON L.: "Theoretical and Experimental Investigation of the Buckling and Post Buckling Characteristics of Flat Carbon Fibre Reinforced Plastics ( CFRP ) Panels Subjected to Compression or Shear Loads". *ICAS* 1978, S.217-223
- [2] KUDVA, N.J.; AGARWAL, B.L.: "Postbuckling Analysis of Stiffened Composite Shear Panels - Theoretical Analysis and Comparison with Experiments". *ICAS* 1981, S.221-229
- [3] ROUSE, M.: "Postbuckling and Failure Characteristics of Stiffened Graphite-Epoxy Shear Webs". *AIAA-87-0733*, (1987)
- [4] ARNOLD, R.R.; PAREKH, J.C.: "Buckling, Postbuckling, and Failure of Stiffened Panels Under Shear and Compression". *J. Aircraft*, Vol. 24(1987), S.803-811
- [5] BUSHNELL, D.: "Nonlinear Equilibrium of Imperfect Locally Deformed Stringer-Stiffened Panels under Combined In-Plane Loads". *Comp. & Struct.*, Vol. 27 (1987), S.519-539
- [6] STEIN, M.: "Postbuckling of Eccentric Open-Section Stiffened Composite Panels". *ICAS-88-5.6.2*, 1988, S.913-919
- [7] SHEINMAN, I.; FROSTIG, Y.: "Post-Buckling Analysis of Stiffened Laminated Panel". *J. Appl. Mechanics*, Vol. 55(1988), S.635-640
- [8] HYER, M.W.; COHEN, D.: "Calculation of Stresses in Stiffened Composite Panels". *AIAA Journal*, Vol. 26 (1988), S.852-857
- [9] ENGBLOM, J.J.; OCHOA, O.O.: "Finite Element Formulation Including Interlaminar Stress Calculation", *Comp. & Struct.*, 9 Vol. 23(1986), S.241-24
- [10] BARSOUM, R.S.; FREESE, C.E.: "An Iterative Approach For The Evaluation Of Delamination Stresses In Laminated Composites". *Int. J. Num. Meth. Eng.*, Vol. 20(1984), S.1415-1431
- [11] RICHTER, H.: "Querfestigkeit bei CFK-Strukturen". *MBB-Report-Nr.: Z-142/87*, Ottobrunn, 1987
- [12] TUNKER, H.: "Comparison of Measured and Computed Load-Deflection-Behaviour of Shear-Loaded Fiber Reinforced Plates in the Postbuckling Range". *ICAS-84-3.4.3*, Toulouse, 1984
- [14] WOLF, K; KOSSIRA, H.: "The Buckling And Postbuckling Behaviour of Curved CFRP Laminated Shear Panels". *ICAS /-88-3.4.3*, (1988)
- [15] WOLF, K; KOSSIRA, H.: "Zur Berechnung des nicht-linearen Tragverhaltens von Strukturen aus Faserverbundwerkstoffen", in: Entwurf und Anwendung von Faserverbundstrukturen, *DGLR-Report 87-02*, Bonn, 1987
- [16] WOLF, K.: "Untersuchungen zum Beul- und Nachbeulverhalten schubbeanspruchter Teilschalen aus Kohlenstoffaserverstärktem Kunststoff", *Dissertation*, TU Braunschweig, 1988
- [17] BEER, G.: "An Isoparametric Joint/Interface Element for Finite Element Analysis". *Int. J. Num. Meth. Eng.*, Vol. 21(1985), S.585-600